J. Meas. Sci. Instrum., 2024, 15(2): 149-156.
DOI: 10.62756/jmsi.1674-8042.2024015
http://jmsi.publish.founderss.cn/
jmsi@nuc.edu.cn

Microsphere phase transmission analysis in microsphere-assisted interferometry lift mode

HONG Yujian, FU Xiaofeng, HU Xiaodong*

State Key Laboratory of Precision Measuring Technology and Instruments, Tianjin University, Tianjin 300072, China

***Corresponding author:** HU Xiaodong (xdhu@tju.edu.cn)

Received: May 10, 2024 **Revised:** May 29, 2024 **Accepted:** June 3, 2024

Abstract: Microsphere-assisted microscopy (MAM) is a technique aimed at enhancing the lateral resolution of optical microscopy, enabling high lateral resolution profile measurement when combined with interferometry. MAM can operate in lift mode, facilitating the selection of regions of interest and expanding the field of view. The analysis of the lifting mode of microspheres in microsphere-assisted interferometry is still insufficient, which affects the longitudinal measurement accuracy of microsphere-assisted interferometry. The phase transmission mechanism of the microsphere was simulated in this paper, and the relationship between the phase distribution below the microsphere and the distance between the microsphere and the sample was summarized. A combined system of microsphere-assisted white light interference microscope was constructed, and the magnification factor and phase distribution of the microsphere in lift mode was measured through atomic force microscope atomic force microscope (AFM) control of the microsphere's position. The experiment validated the simulated results of microsphere phase transmission, providing a theoretical foundation for microsphere-assisted interferometry (MAI) in lift mode.

Key words: microsphere-assisted microscopy (MAM); microsphere-assisted interferometry (MAI); phase transmission; lift mode; optical simulation

0 Introduction

Microsphere-assisted microscopy (MAM) is a method aimed at enhancing the lateral resolution of optical microscopy, characterized by its simplicity of implementation and compatibility with other optical systems[1,2]. In 2011, MAM was first proposed, wherein the silica microspheres with diameter of 2 μm—9 μm were placed on the sample surface to enhance the optical system's lateral resolution[3]. Under visible light illumination, structures with minimum feature sizes as small as 50 nm can be resolved. The diameter[4], material[5], immersion depth[6], and illumination[7] of microspheres[8] were analyzed, and the microspheres[9,10] were modified, thus enhancing the resolution capability of MAM. This capability leads to the widespread application of MAM in fields such as microstructure fabrication and life sciences.

To broaden the application of MAM, manipulation techniques such as transparent thin films[5], optical tweezers[11,12], and cantilevers[8,13,14] are adopted to control the three-dimensional position of the microspheres. It enables microspheres to operate in a lift mode above the sample surface, reducing sample invasiveness while facilitating field-of-view stitching. However, the aforementioned efforts have been limited to measuring two-dimensional information of samples. In practical applications, there is a growing demand for acquiring the three-dimensional profile of samples to achieve more comprehensive measurements of microstructures.

MAM is combined with traditional interferometric techniques such as digital holography[15,16], phase-shifting interferometry[17,18], and white-light interferometry (WLI)[19] to obtain high lateral resolution surface profile information. However, these studies merely place microspheres on the sample surface or integrate them with the objective[20], without controlling the microspheres to achieve measurements in the lift mode. In addition, the analysis of the phase transmission mechanism of the microsphere is less, which leads to the influence of the microsphere in the interferometric system, and the measurement of the sample height information is not accurate.

To address these issues, Comsol multiphysics and Zemax optics studio were employed to simulate the phase transmission of the microsphere, exploring its phase distribution. The variable of the distance between the microsphere and the sample was introduced, and the relationship among the width of the microsphere center phase transition area (CPTA), the maximum phase difference, and the distance between microspheres and samples is established. A system combining MAM with WLI was constructed and the magnification factor of the microsphere and the phase distribution beneath microspheres relative to the distance between the microsphere and the sample was measured through atomic force microscope (AFM) manipulation of microspheres' three-dimensional position. The experimentally obtained phase distribution validated the simulation results, thereby mutually reinforcing each other. The simulations and experiments presented in this paper laid a foundation for improving the height measurement accuracy of microsphere-assisted interferometry (MAI) and for implementing MAI in the lift mode.

1 Simulation of microsphere phase transmission

In order to investigate the phase transmission mechanism of microspheres, the phase distribution of microspheres was simulated from the perspectives of wave optics and geometric optics, and the similarities and differences between the two simulation methods were compared.

1.1 Wave optics

Currently, in the combination of MAM and interferometry, the primary material used was silica, with diameters typically in the tens of micrometers to ensure adequate imaging field for microspheres. Therefore, the silica microsphere with a diameter of 50 μm was selected in the simulation. Fig. 1 presents the simulation results of the optical electric field intensity distribution and phase distribution of the microsphere using Comsol multiphysics. As the experimental illumination source in the experiment sections was white light with a central wavelength of 570 nm, employing Köhler illumination, the simulation adopted collimated light with a wavelength of 570 nm from the top of the region to illuminate the microsphere. Perfectly matched layers (PML) with a thickness of one wavelength were added around the simulation region to simulate a more realistic distribution of the optical field. The simulation region was set to be 60 μm×100 μm to accommodate a microsphere with a diameter of 50 μm and demonstrate its ability to focus the light beam.

Fig. 1(a) shows the distribution of the electric field intensity after collimated light enters the microsphere. The collimated light focused beneath the microsphere, forming the nanojet. Fig. 1(b) shows the phase distribution after the collimated light enters the microsphere. It could be observed that the phase distribution was uniform before passing through the microsphere, whereas significant phase changes occurred beneath the microsphere. The phase beneath the microsphere could be divided into two regions: above and below the focal point. Above the focal point, the phase distribution was complex, while below the focal point, it resembled the phase distribution formed by a point source of light at the focal point.

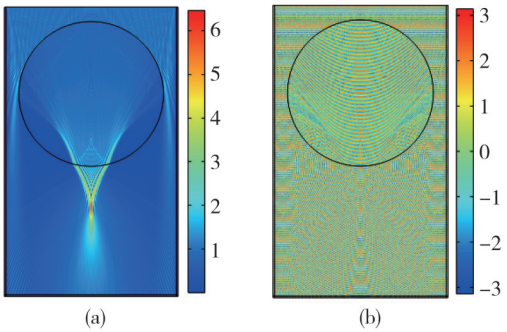

Fig. 1 Simulation results from Comsol multiphysics. (a) Electric field intensity distribution; (b) Phase distribution

Fig. 2(a), (c), (e) shows the phase distribution curves beneath the microsphere at distances of 0 nm, 500 nm, and 1 000 nm, respectively. Due to the illumination wavelength of 570 nm and the observation range of 50 μm, the phase changes were dense, making it difficult to discern intuitive trends. Therefore, phase unwrapping were performed by Matlab unwrap function of Fig. 2(a), (c), (e) to obtain Fig. 2(b), (d), (f), respectively. The results indicated that as the observation position moved away from the center of the microsphere, the phase curve exhibited a trend of initially increasing and then decreasing. The region where the phase increased with the distance from the center of the microsphere was called CPTA. From the simulation results of microsphere phase transmission, it was evident that the phase distribution beneath the microsphere was not merely a spherical envelope curve but rather the result of the complex transmission of light through the microsphere.

When the microsphere is used for imaging, the available imaging area of the microsphere typically does

not exceed its own size. Considering that the magnification factor of microspheres is usually between 2.5 to 4, and from experimental experience, it can be determined that the usable field of view for a 50 μm diameter microsphere is approximately half of the microsphere's diameter when viewed in the CCD. Assuming a minimum magnification of 2.5 times, the actual imaging field of view is calculated to be 10 μm. The calculation showed that the usable field of view of the microsphere was within the CPTA range. Therefore, the analysis of the CPTA was of significant importance.

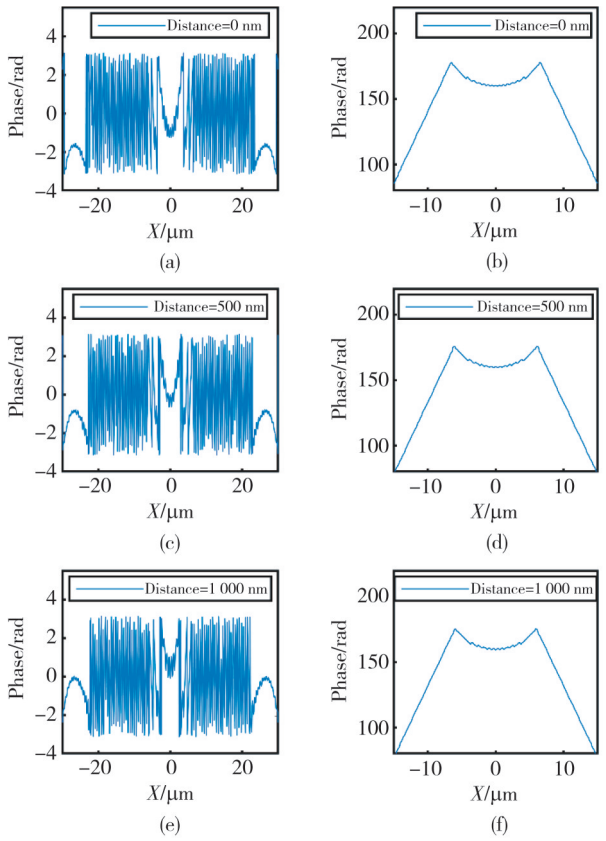

Fig. 2 Phase distribution below microsphere. (a) Phase distribution at a distance of 0 nm; (b) Unwrapped result of (a); (c) Phase distribution at a distance of 500 nm; (d) Unwrapped result of (c); (e) Phase distribution at a distance of 1 000 nm; (f) Unwrapped result of (e)

From Fig.2(b), (d), (f), it can be observed that the phase variation within this region forms relatively smooth curves. Two parameters were used to describe the characteristics to depict the trend of the region's variation: the width of CPTA and the phase difference between the center and the edge. The CPTA of the microsphere varies with the distance between the microsphere and the sample, as shown in Fig.3.

As shown in Fig.3(a), the phase difference within the CPTA exhibits an oscillating decreasing trend with increasing distance of the microsphere from the sample surface. It indicated that as the microsphere moved further away from the sample surface, the phase difference between the center and the edge decreased, and the phase distribution beneath the microsphere changed more gradually. From the perspective of microsphere phase distribution, it was evident that the microspheres were more suitable for interference measurements in the lift mode. The width of the central region decreases as the distance between the microsphere and the sample increases, as shown in Fig. 3(b). It was because the influence of the microsphere on the optical field below primarily concentrates in the central region. As the observation plane approached the focal point of the microsphere with the increase in distance between the observation plane and the microsphere, the width of the CPTA decreased.

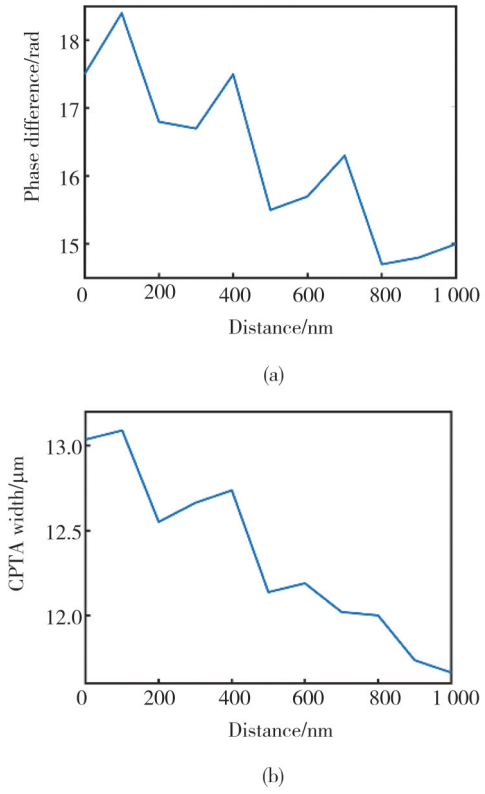

Fig. 3 Relationship between phase difference and distance, CPTA width and datance. (a) Relationship between phase difference and distance; (b) Relationship between CPTA width and distance

1.2 Geometric optics

Zemax optics studio was employed to simulate the phase distribution beneath the silica microsphere with a diameter of 50 μm, aiming to compare the differences between wave optics and geometric optics simulation methods. Fig. 4 depicts a schematic diagram of the

simulation, where collimated light with a wavelength of 570 nm is incident from the left side through an aperture onto the microsphere and impinges on the object surface. The sampling of the incident light is set to 4 096 pixels× 4 096 pixels. Both the aperture and the microsphere are set with an aperture diameter of 25 μm, and the microsphere is made of silica. The object surface, acting as the observation plane, was closely positioned beneath the microsphere.

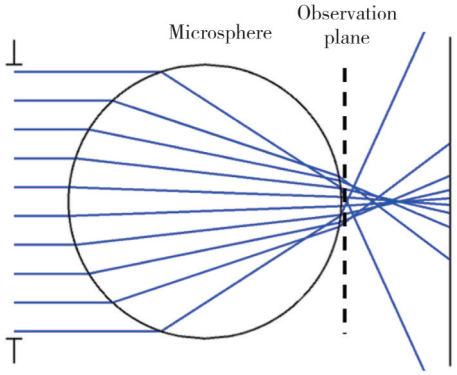

Fig. 4 Zemax optics studio simulation

The phase distribution on the observation plane beneath the microsphere is illustrated in Fig.5. Before unwrapping, the phase appeared somewhat chaotic, but it's apparent that the phase variation was smoother compared to the results simulated using Comsol multiphysics. Moreover, aside from the CPTA, the phase variation on the periphery did not reach π. Fig.5(b) presents the phase distribution after unwrapping the phase distribution curve from Fig.5(a). Although the phase variation trend simulated by Zemax optics studio was similar to that of Comsol multiphysics, both exhibiting a CPTA, the width of the CPTA and the phase difference between the center and the edge were not identical. The phase variation simulated by Zemax optics studio appeared to be smoother.

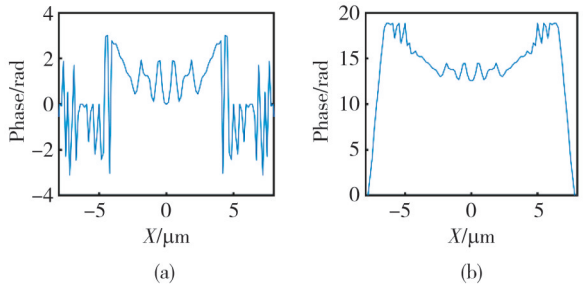

Fig. 5 Phase distribution simulation results from Zemax optics studio. (a) Phase distribution at a distance of 0 nm; (b) Unwrapped result of (a)

Zemax exhibited a phase distribution trend similar to Comsol, although their values differed, primarily due to two reasons. Firstly, the simulation employed microsphere diameters in the micron range and visible light wavelength, while Zemax was more commonly used for geometric optics simulations. The reliability of phase distribution simulations at this scale in Zemax may not match those conducted with wave optics simulations using Comsol. It was evident from the width of the phase simulation results in Zemax, where the *X*-axis direction exhibited finer regions, and the analysis primarily focused on positions of concentrated light intensity while neglecting the edge regions. Secondly, considering the limitations of simulation conditions, the sampling rate of the collimated light source may introduce errors to the simulation. Nevertheless, the simulation results from Zemax confirmed the trends observed in the Comsol simulation results.

2 Experiments

To verify the phase distribution of the microsphere in the lift mode, a combined system of MAM and WLI is constructed, as illustrated in Fig.6.

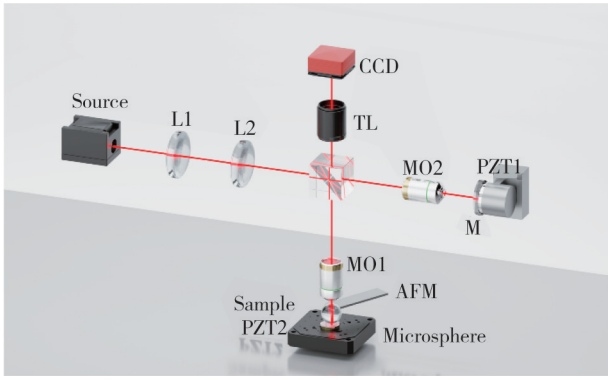

Fig. 6 Microsphere-assisted white-light interferometry system (Position of microsphere is precisely controlled by AFM)

The system mainly consisted of white light interference microscope and AFM[21]. The system adopted a Linnik configuration to ensure the working distance of the objective lens, and the illumination source was a white-light source with a central wavelength of 570 nm. L1 was a collimating lens that adjusted the white-light source to parallel light. L2 was a Köhler illumination lens, which ensured that the illuminating light was parallel to the sample, along with the objective MO1 and MO2 positioned behind it. A 50:50 visible light wavelength beamsplitter was used to ensure the quality of interference between object light and reference light. Two 10× objective lenses MO1 and MO2 were placed in the object light path and reference light path, respectively. Their positions were precisely adjusted to ensure the symmetry of the interference light path. A tube lens TL was installed on the camera to ensure that the CCD collected the sample image. The

reference mirror M was placed on the piezo actuator PZT1 to achieve WLI scanning, with a step distance of 20 nm between images. The sample was positioned on the displacement stage of the AFM to achieve focusing and selection of the region of interest.

The microsphere was adhered to the AFM by nano-manipulation[22]. By engaging, the microsphere can reach the sample, and by adjusting the piezo actuator PZT2 of the AFM, the microsphere can be lifted from the sample surface. Both the lowering and lifting operations were performed under the feedback of the AFM to ensure the accuracy of microsphere position control. The structure of the microsphere and AFM is depicted in Fig.7, where the microsphere is adhered to the side of the cantilever to allow the illuminating light to pass through the microsphere for imaging.

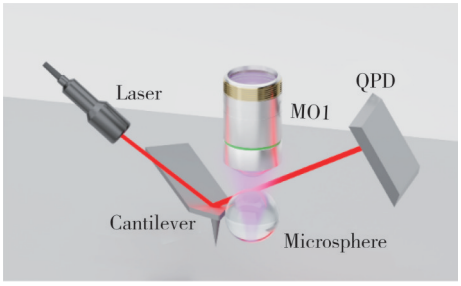

Fig. 7 Structure of microsphere probe and laser path of AFM

To investigate the imaging quality of MAM in lift mode, the USAF 1951 standard resolution target (2017a_USAF_Dmnd, Ready Optics) was used as the sample. The constructed system was employed to test the magnification of the microsphere when the sample was at different distances, ranging from 0 nm to 1 000 nm with intervals of 50 nm. Fig. 8 displays the imaging of the standard resolution target Group 9 Element 6 captured by MAI. It was evident that the standard resolution target with line width of 548 nm and period of 1 096 nm could be easily resolved by the microsphere.

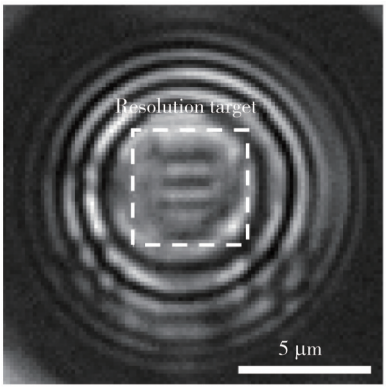

Fig. 8 Image of standard resolution target

Fig. 9 presents the measurement results of the magnification when the microsphere is lifted from the sample. The magnification of the microsphere is calculated as the ratio of the magnification of the imaging system with the microsphere to that without the microsphere. Due to the presence of certain aberrations and distortions in the microsphere and the fact that the magnification at the edge region may differ from that at the center region, the magnification measurement only considers the central region of the microsphere.

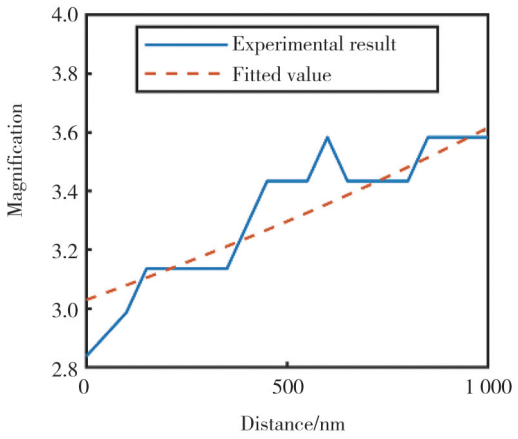

Fig. 9 Relationship between magnification of microsphere and distance

When the microsphere is lifted from the sample, the magnification should follow a relatively smooth curve. However, in actual measurements, the magnification is calculated based on the number of pixels corresponding to the periodicity of the resolution target in the field of view. Since the feature size of the standard resolution target used for calibration was small of the system, with each line width being only about 5 pixels, the magnification values were not continuous. Moreover, since the position of the virtual image plane also changed when the microsphere was lifted from the sample, it was necessary to refocus each time when the microsphere position was adjusted. Considering the limited depth of field of the objective lens, inaccurate focusing may introduce some errors. Therefore, the measurement results in Fig.9 appear as a broken line.

The magnification of the microsphere is fit using virtual image theory[23], as shown by the dashed line in Fig. 9. It could be seen that the measured magnification of the microsphere aligned well with the theory of virtual image magnification. Magnification is a crucial parameter for imaging and interferometric measurements using the microsphere, as it directly affects the accuracy of lateral measurements in MAI. Additionally, according to the theory of virtual image magnification,

the magnification of the microsphere also influenced its super-resolution capability. Investigating the variation of magnification as the microsphere is lifted from the sample surface helps analyze the microsphere's optimal working position.

The phase transmission mechanism of the microsphere is crucial in the application of MAM in interference systems. The phase distribution of the microsphere in lift mode is measured using a standard plane as the sample, and the results are shown in the Fig. 10. Fig. 10(a) depicts the white light interference fringes of the microsphere at the standard plane. During the process of raising the microsphere, the interference fringes changed subtle change. Fig. 10(b), (c), (d) display the phase distribution obtained at distances of 0 nm, 500 nm, and 1 000 nm, respectively. It could be observed that the phase error introduced by the microsphere exhibited a centrally symmetric distribution with smaller phase errors in the central region and larger errors away from the central region, similar to the simulation results.

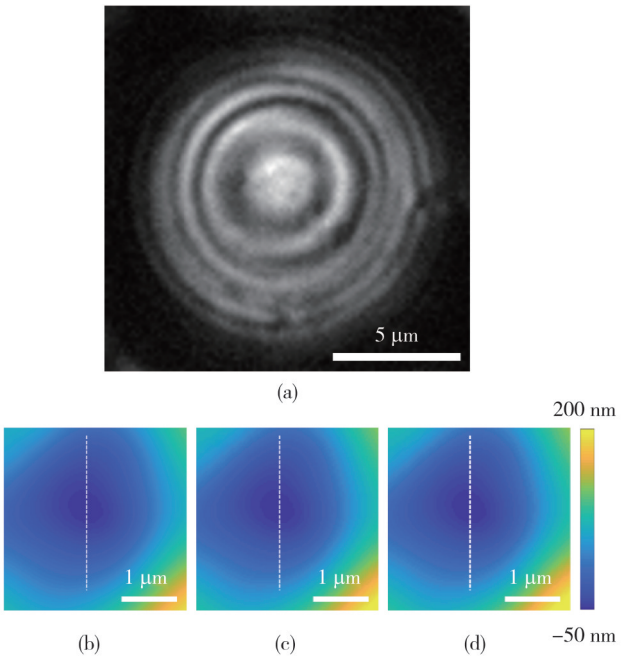

Fig. 10 Measurement of phase distribution of microsphere. (a) MAI imaging of a standard plane; (b–d) Phase distribution of microsphere at distances of 0 nm, 500 nm, and 1 000 nm

As the distance between the microsphere and the sample increased, the phase distribution did not exhibit significant changes. For a 50 μm microsphere, the changes in the range of 0 nm—1 000 nm could not be distinctly visualized in the parula colormap. Fig. 11 presents the height curve results from Fig. 10(b), (c), (d) which undergo Gaussian first-order blurring to remove noise. The three curves are aligned based on the lowest point of the central phase to facilitate better comparison. The overall trend of the phase distribution curves exhibited a symmetrical pattern around the microsphere center, with the rate of phase variation increasing as one moved away from the central region. The farther the microsphere was from the sample, the faster the phase distribution changed, and the greater the difference between the phase at the edge and the center, resulting in narrower curve openings. When the microsphere was raised to a distance of 1 000 nm, the phase error at a distance of 1.5 μm from the central sample reached 20 nm, with no significant impact on the central trend.

In the optimal imaging area of the microsphere, namely the central region of the microsphere, the measurement results of microsphere-assisted interference measurements were not sensitive to the distance between the microsphere and the sample, while the edge region was more affected. In Fig. 11, the phase distribution curve of the microsphere is fit at a distance of 0 nm from the sample using circular functions. The fitting results showed that although the phase distribution curve of the microsphere was similar to a circle, it was not exactly the same. The phase distribution curve of the microsphere's edge increased more rapidly than that of the circular function, which was consistent with the simulation results.

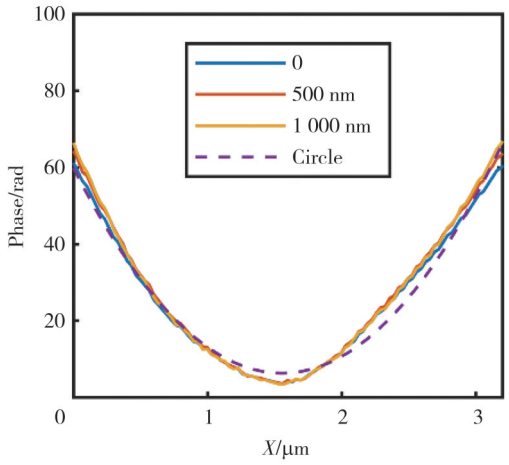

Fig. 11 Phase distribution curves of microsphere at different distances and circular fitting results. This figure presents profile results of phase distribution shown in Fig. 10(b–d)

MAM were combined with WLI to successfully measure the phase distribution of the microsphere under lift mode, validating the simulation results, providing guidance for MAI. As the microsphere was lifted, both the magnification factor and the phase transmission of the microsphere changed with the distance between the microsphere and the sample, affecting the accuracy of

lateral width and vertical height measurements of the sample. Comprehensive analysis of various influences of the distance between the microsphere and the sample helps determined the optimal working distance of the microsphere, thereby enhancing the measurement capability of MAI.

3 Conclusions

Lift mode was explored in MAI, and the phase transmission mechanism of the microsphere was simulated from both wave optics and geometric optics perspectives. The relationship between the phase distribution beneath the microsphere and the distance between the microsphere and the sample was analyzed. It could be summarized that the width of the CPTA decreased with increasing distance, and the phase difference between the center and the edge decreased with increasing distance. A MAM-WLI integrated system was constructed, the microsphere was introduced into the interference optical path, and AFM was used to control the distance between the microsphere and the sample. This enabled the determination of the magnification factor and phase distribution of the microsphere and their relationship with the distance between the microsphere and the sample, thereby validating the simulation results and laying the groundwork for further development of MAI.

Acknowledgement

This work was supported by National Natural Science Foundation of China (No.52275540).

Declaration of conflicting interests

The authors have no conflict of interests related to this publication.

References

[1] YAN Y Z, LI L, FENG C, et al. Microsphere-coupled scanning laser confocal nanoscope for sub-diffraction-limited imaging at 25 nm lateral resolution in the visible spectrum. ACS Nano, 2014, 8(2): 1809-1816.

[2] HAO X, KUANG C F, LIU X, et al. Microsphere based microscope with optical super-resolution capability. Applied Physics Letters, 2011, 99(20): 203102.

[3] WANG Z, GUO W, LI L, et al. Optical virtual imaging at 50 nm lateral resolution with a white-light nanoscope. Nature Communications, 2011, 2(1): 218.

[4] DARAFSHEH A, WALSH G F, NEGRO L D, et al. Optical super-resolution by high-index liquid-immersed microspheres. Applied Physics Letters, 2012, 101(14): 141128.

[5] DARAFSHEH A, GUARDIOLA C, PALOVCAK A, et al. Optical super-resolution imaging by high-index microspheres embedded in elastomers. Optics Letters, 2015, 40(1): 5-8.

[6] LEE S, LI L, WANG Z B, et al. Immersed transparent microsphere magnifying sub-diffraction-limited objects. Applied Optics, 2013, 52(30): 7265-7270.

[7] LIU C, YE A P. Microsphere assisted optical super-resolution imaging with narrowband illumination. Optics Communications, 2021, 485: 126658.

[8] WANG F F, LIU L Q, YU H B, et al. Scanning superlens microscopy for non-invasive large field-of-view visible light nanoscale imaging. Nature Communications, 2016, 7: 13748.

[9] WU M X, HUANG B J, CHEN R, et al. Modulation of photonic nanojets generated by microspheres decorated with concentric rings. Optics Express, 2015, 23(15): 20096-20103.

[10] ZHOU Y, JI R, TENG J H, et al. Wavelength-tunable focusing via a Fresnel zone microsphere. Optics Letters, 2020, 45(4): 852-855.

[11] XI L, HU S, TANG Y. Coated high-refractive-index Barium titanate glass microspheres for optically trapped microsphere super-resolution microscopy: a simulation study. Photonics, 2020, 7(4): 84.

[12] ZHAI C, HONG Y, LIN Z, et al. An optical tweezer-based microdroplet imaging technology. Nanotechnology and Precision Engineering, 2023, 6(3): 033004.

[13] KRIVITSKY L A, WANG J J, WANG Z B, et al. Locomotion of microspheres for super-resolution imaging. Scientific Reports, 2013, 3: 3501.

[14] ZHOU J, LIAN Z, ZHOU C, et al. Scanning microsphere array optical microscope for efficient and large area super-resolution imaging. Journal of Optics, 2020, 22(10): 105602.

[15] WANG Y X, GUO S, WANG D Y, et al. Resolution enhancement phase-contrast imaging by microsphere digital holography. Optics Communications, 2016, 366: 81-87.

[16] AAKHTE M, ABBASIAN V, AKHLAGHI E A, et al. Microsphere-assisted super-resolved Mirau digital holographic microscopy for cell identification. Applied Optics, 2017, 56(9): D8-D13.

[17] PERRIN S, LEONG-HOÏ A, LECLER S, et al. Microsphere-assisted phase-shifting profilometry. Applied Optics, 2017, 56(25): 7249.

[18] STEPHANE P, DONIE YIDENEKACHEW J, PAUL M, et al. Compensated microsphere-assisted interference microscopy. Physical Review Applied, 2020, 13(1): 014068.

[19] WANG F, LIU L, YU P, et al. Three-dimensional super-resolution morphology by near-field assisted white-light interferometry. Scientific Reports, 2016, 6(1): 24703.

[20] YAN B, WANG Z B, PARKER A L, et al. Superlensing microscope objective lens. Applied Optics, 2017, 56(11):

3142-3147.
[21] LU N H, XIAO S S, ZHANG R, et al. Thin head atomic force microscope for integration with optical microscope. The Review of Scientific Instruments, 2022, 93(8): 083702.
[22] HONG Y J, XIAO S S, ZHAI C, et al. Microsphere probe: combining microsphere-assisted microscopy with AFM. Optics Express, 2023, 31(17): 27520-27528.
[23] CHEN L W, ZHOU Y, LI Y, et al. Microsphere enhanced optical imaging and patterning: From physics to applications. Applied Physics Reviews, 2019, 6(2): 021304.

微球辅助干涉术抬起模式下微球相位传输分析

洪羽剑, 付晓锋, 胡晓东*

天津大学 精密测试技术及仪器全国重点实验室, 天津 300072

摘　要: 微球辅助显微术是一项提升光学显微系统横向分辨力的技术, 可与传统干涉技术结合以实现高横向分辨力的三维形貌测量。微球可工作于抬起模式下, 进行感兴趣区域的选取与视场扩展。现有研究对微球辅助干涉术中微球工作在抬起模式时的分析仍不充分, 影响了微球辅助干涉技术的纵向测量精度。本文对微球的相位传输机制进行了仿真, 总结了微球下方相位分布与微球和样品距离之间的关系。同时, 搭建了微球-白光干涉联用系统, 并通过AFM控制微球的三维位置, 对微球抬起模式下的放大倍数与相位分布进行测量, 验证了仿真中微球下方相位分布的结果, 为微球辅助干涉术中抬起模式提供了理论基础。

关键词: 微球辅助显微术; 微球辅助干涉术; 相位传输; 抬起模式; 光学仿真

引用格式: HONG Yujian, FU Xiaofeng, HU Xiaodong. Microsphere phase transmission analysis in microsphere-assisted interferometry lift mode. Journal of Measurement Science and Instrumentation, 2024, 15(2): 149-156.